

NMR HRMAS Spectroscopy of Lung Biopsy Samples: Comparison Study Between Human, Pig, Rat, and Mouse Metabolomics

Malika A. Benahmed,^{1,2} Karim Elbayed,² François Daubeuf,³
Nicola Santelmo,⁴ Nelly Frossard,³ and Izzie J. Namer^{1,5*}

Purpose: Using the metabolomics by NMR high-resolution magic angle spinning spectroscopy, we assessed the lung metabolome of various animal species in order to identify the animal model that could be substituted to human lung in studies on fresh lung biopsies.

Methods: The experiments were conducted on intact lung biopsy samples of pig, rat, mouse, and human using a Bruker Advance III 500 spectrometer. Thirty-five to 39 metabolites were identified and 23 metabolites were quantified. Principal component analysis, partial least-squares discriminant analysis, and analysis of variance tests were performed in order to compare the metabolic profiles of each animal lung biopsies to those of the human lung.

Results: The metabolic composition between human and pig lung was similar. However, human lung was distinguishable from mouse and rat regarding: Trimethylamine *N*-oxide and betaine which were present in rodents but not in human lung, carnitine, and glycerophosphocholine which were present in mouse but not in human lung. Conversely, succinic acid was undetected in rat lung. Furthermore, fatty acids concentration was significantly higher in rodent lungs compared to human lung.

Conclusion: Using the metabolomics by NMR high-resolution magic angle spinning spectroscopy on lung biopsy, samples allowed to highlight that pig lung seems to be close to human lung as regarding its metabolite composition with more similarities than dissimilarities. **Magn Reson Med 71:35–43, 2014.**
© 2013 Wiley Periodicals, Inc.

Key words: lung; metabolomics; NMR HRMAS

Metabolomics ¹H high-resolution magic angle spinning (HRMAS) NMR spectroscopy is a technique used for the measurement of low metabolite levels directly on intact tissues in both normal and pathological conditions, influenced by the environment or drug exposure (1,2). This is an original technique for the identification of potential biomarkers for diagnosis or prognosis that has become increasingly useful for the study of several diseases (3–8). Metabolomics has also become applicable in the monitoring of the quality of organ transplants, because metabolic changes occur very quickly in nonvascularized tissue (9). Metabolomics offers a rapid and inexpensive tool to monitor organ viability or to detect organ rejection (10,11). However, very few papers in the literature combine the use of the metabolomics by HRMAS NMR spectroscopy directly on intact tissue for lung transplantation (12) and most publications assess the metabolome of the lung using biofluids (13–15).

The translation from basic biomedical knowledge to prevention and treatment of human diseases requires use of animal models, as for developments that cannot be tested in humans for practical or evident ethical reasons. In this regard, there is a growing interest in the use of metabolomics NMR techniques to explore lung biopsy samples of animal models for transplantation (9,16), inflammation, and lung injury (17–19).

This study compares the metabolic profiles of fresh lung biopsy samples obtained from humans to those of the lung from the most useful animal models for lung exploration, i.e., pigs, mice, and rats, using metabolomics HRMAS NMR spectroscopy with the purpose of identifying the most suitable animal model for the exploration of respiratory diseases.

METHODS

Tissue Collection

Patient Population

This study involves use of human lung biopsy samples obtained from the University Hospital of Strasbourg (Centre de Ressources Biologiques, Hôpitaux Universitaires de Strasbourg) between July 2009 and August 2011 in accordance with French legislation. Eleven samples collected from six patients were used in this study (six males; mean age, 68 ± 12 years; range, 55–80 years). All patients underwent a surgical procedure with no chemotherapy or radiotherapy treatment. During lung cancer

¹Faculté de Médecine, Laboratoire d'Imagerie et de Neurosciences Cognitives (LINC), Institut de Physique Biologique, Université de Strasbourg/CNRS UMR7237, Strasbourg Cedex, France.

²Laboratoire de RMN et Biophysique des membranes, Institut de Chimie, Université de Strasbourg/CNRS UMR7177, Strasbourg, France.

³Laboratoire d'Innovation Thérapeutique, Faculté de Pharmacie, Université de Strasbourg/CNRS UMR 7200, Illkirch, France.

⁴Service de Chirurgie Thoracique, Nouvel Hôpital Civil, Hôpitaux Universitaires de Strasbourg, Strasbourg, France.

⁵Service de Biophysique et Médecine Nucléaire, Hôpital de Hautepierre, Hôpitaux Universitaires de Strasbourg, Strasbourg Cedex 09, France.

*Correspondence to: Izzie J. Namer, M.D., Ph.D., Service de Biophysique et Médecine Nucléaire, Hôpital de Hautepierre, Hôpitaux Universitaires de Strasbourg, 1 avenue Molière, Strasbourg Cedex 67098, France. E-mail: izzie.jacques.namer@chru-strasbourg.fr

Received 24 May 2012; revised 3 January 2013; accepted 3 January 2013
DOI 10.1002/mrm.24658

Published online 14 February 2013 in Wiley Online Library (wileyonlinelibrary.com).

surgery, a total lobectomy was performed; the healthy biopsy tissues were collected within the lobectomy and then were examined by histopathology. The lung biopsies were collected rapidly, reducing the ischemic delay as much as possible after resection (less than 2 min). Biopsies were immediately frozen on dry ice and kept at -80°C until NMR measurements.

Animal Handling and Experimental Protocol

The experimental protocol was conducted in accordance with our research committee guidelines based on the French ethics regulations and was granted authorization by the CREMEAS (Regional Committee for Ethics in Experimentation Using Animals).

Pigs. Seven large White pigs (mean weight, 27 ± 4 kg) were used, housed in the animal facility at Institut de Recherche contre les Cancres de l'Appareil Digestif (Hôpitaux Universitaires de Strasbourg, France). Premedication was intramuscular ketamine (50 mg/kg) and azaperone (2 mg/kg), followed by intravenous induction of general anesthesia with propofol (3 mg/kg). Tracheal intubation was facilitated with pancuronium (0.2 mg/kg). Anesthesia was maintained with isoflurane and nitrous oxide (Abbott, Rungis, France) in 50% oxygen. Lung samples at baseline were taken in heart-beating animals before induction of cardiac arrest. Samples were snap frozen on dry ice and kept at -80°C until the measurements were taken.

Mice. Eleven BALB/c mice with a mean weight of 28 ± 5 g were used. They were housed in the animal facility at the Pharmacy Faculty (Université de Strasbourg, Illkirch, France) and maintained at room temperature (22°C) under a 12 h/12 h normal light/dark cycle, with food and water ad libitum. The general anesthesia was given using intraperitoneal induction of ketamine (154 mg/kg) (Imalgene 1000, MERIAL, Lyon, France) and xylazine (10 mg/kg) (Rompun, Bayer HealthCare) with a 6 mL/kg flow rate.

Rats. Eleven adult male Wistar rats were selected at 8 weeks of age (mean weight, 250 g). The animals were housed at the animal facility at the Pharmacy Faculty (Université de Strasbourg, Illkirch, France) and maintained at room temperature (22°C) under a 12 h/12 h normal light/dark cycle, with food and water ad libitum. The rats were anesthetized using an intraperitoneal injection of ketamine (80 mg/kg) and xylazine (4 mg/kg).

For mouse and rat, the baseline left and right lungs were collected from surgical specimens directly at surgery, immediately snap-frozen in liquid nitrogen, and stored at -80°C until NMR analysis.

Sample Preparation for NMR Spectroscopy Analysis

Each lung biopsy sample was prepared at -20°C as previously described (9,20) by placing a 15–20 mg biopsy into a disposable 30 μL Kelf insert. To provide a lock frequency for the NMR spectrometer, 10 μL of D_2O was also added to the insert. The insert was then sealed tightly and stored at -80°C until the HRMAS analysis. Shortly before the HRMAS analysis, the insert was placed in a standard 4 mm ZrO_2 rotor and closed with a cap. The ensemble was then introduced into a HRMAS probe precooled at 4°C .

NMR HRMAS Spectroscopy

All NMR experiments were conducted on intact biopsy samples spinning at 3502 Hz recorded on a Bruker Advance III 500 spectrometer operating at a proton frequency of 500.13 MHz fitted with Bruker TopSpin software (Bruker Biospin). The spectrometer is equipped with a 4-mm double-resonance (^1H , ^{13}C) gradient HRMAS probe. A Bruker cooling unit maintains the temperature at 4°C . The major advantage of conducting experiments at low temperature is to limit the degradation of the sample during the short acquisition time (20 min) (21,22).

For each biopsy sample, a 1D ^1H spectrum using a one-pulse experiment followed by a Carr-Purcell-Meiboom-Gill (CPMG) pulse sequence was acquired as reported elsewhere (9,23). The CPMG sequence is adequate to reduce the intensity of lipid signals and macromolecules to the level of the metabolites in tissues (20,24). The inter-pulse delay between the 180° pulses of the CPMG pulse train was synchronized with the sample rotation and set to 285 μs ($1/\omega = 1/3502 = 285 \mu\text{s}$) in order to eliminate signal losses due to B_1 inhomogeneities. The number of loops was set to 328, giving the CPMG pulse train a total length of 93 ms. The parameters for the CPMG experiment were: sweep width, 14.2 ppm; number of points, 32k; relaxation delay, 2 s; and acquisition time, 2.3 s. A total of 128 free induction decays were acquired resulting in an acquisition time of 10 min. The free induction decay was multiplied by an exponential weighing function corresponding to a line broadening of 0.3 Hz before Fourier transformation. All spectra were referenced by setting the lactate doublet chemical shift to 1.33 ppm.

Two-dimensional (2D) heteronuclear spectra were acquired to aid the identification of metabolites. ^1H - ^{13}C phase-sensitive detection (echo/antiecho) heteronuclear single quantum correlation was performed using a 73-ms acquisition time with globally optimized alternating phase rectangular pulse ^{13}C decoupling and a 1.5 s relaxation delay. A total of 116 transients were averaged for each of the 256- t_1 increments (for a total acquisition time of 15 h) (9,23). However, 2D experiments of such a long duration may lead to tissue degradation, resulting in an increased concentration for some metabolites (e.g., creatine, choline, phosphocholine, etc.) (21,22). For this reason, 2D experiments are only used for signal assignment. For each sample, we used the above-described parameters according to the following sequence of acquisition: 1D one-pulse acquisition for 10 min followed by a CPMG sequence for 10 min (11 spectra per animal species) and 2D (heteronuclear single quantum correlation) acquisition for 15 h (a total of 18 spectra).

A total of 35 metabolites were identified from the spectra obtained for the human and pig lung samples, 36 metabolites for rat lung samples, and 39 metabolites for the mouse lung samples (Table 1; Figs. 1 and 2).

Quantitative NMR Metabolomics

Metabolites were quantified using the 1D CPMG spectra except for fatty acid quantification for which a one-pulse sequence was used.

Table 1
Metabolite Composition of Lung Biopsy Samples (nmol/mg Tissue) and the ANOVAs Followed by the Dunnett's Tests

Compound	Concentrations Mean \pm SD (nmol/mg)						Statistics		
	Humans	Pigs	Rats	Mice	ANOVA	Humans vs. pigs	Humans vs. rats	Humans vs. mice	
						$P < 0.05$	$P < 0.05$	$P < 0.05$	
1 Acetate	0.060 \pm 0.008	0.031 \pm 0.003	0.032 \pm 0.005	0.013 \pm 0.002	$P < 0.0001$	$P < 0.05$	$P < 0.05$	$P < 0.05$	
2 Alanine	0.42 \pm 0.05	0.52 \pm 0.04	0.66 \pm 0.06	0.28 \pm 0.03	$P < 0.0001$	ns	$P < 0.05$	ns	
3 Arginine	+	+	+	+					
4 Ascorbate	0.20 \pm 0.02	0.44 \pm 0.04	0.43 \pm 0.05	0.41 \pm 0.04	$P < 0.001$	$P < 0.05$	$P < 0.05$	$P < 0.05$	
5 Asparagine	2.2 \pm 0.2	3.23 \pm 0.24	2.45 \pm 0.20	0.77 \pm 0.078	$P < 0.0001$	$P < 0.05$	ns	$P < 0.05$	
6 Aspartate	+	+	+	+					
7 Betaine	ud	ud	+	+					
8 Choline	0.14 \pm 0.02	0.19 \pm 0.02	0.60 \pm 0.07	0.15 \pm 0.02	$P < 0.0001$	ns	$P < 0.05$	ns	
9 Carnitine	ud	ud	ud	+					
10 Creatine	0.17 \pm 0.03	0.29 \pm 0.01	0.19 \pm 0.02	0.15 \pm 0.02	$P < 0.001$	$P < 0.05$	ns	ns	
11 Ethanolamine	0.12 \pm 0.009	0.11 \pm 0.01	0.18 \pm 0.02	0.17 \pm 0.01	$P < 0.001$	ns	$P < 0.05$	ns	
12 Fatty acids (total CH ₃) one pulse sequence	10.06 \pm 0.78	8.34 \pm 0.55	21.67 \pm 2.67	22.83 \pm 2.58	$P < 0.0001$	ns	$P < 0.05$	$P < 0.05$	
13 Glucose	2.20 \pm 0.09	1.40 \pm 0.15	1.16 \pm 0.08	1.90 \pm 0.12	$P < 0.0001$	$P < 0.05$	$P < 0.05$	ns	
14 Glutamate	1.33 \pm 0.10	2.70 \pm 0.20	1.92 \pm 0.13	0.84 \pm 0.03	$P < 0.0001$	$P < 0.05$	$P < 0.05$	$P < 0.05$	
15 Glutamine	0.42 \pm 0.04	0.18 \pm 0.02	0.22 \pm 0.02	0.40 \pm 0.03	$P < 0.0001$	$P < 0.05$	$P < 0.05$	ns	
16 Glutathione	0.15 \pm 0.01	0.29 \pm 0.02	0.22 \pm 0.01	0.26 \pm 0.02	$P < 0.0001$	$P < 0.05$	$P < 0.05$	$P < 0.05$	
17 Glycerol	+	+	+	+					
18 Glycerophosphocholine	ud	ud	ud	0.58 \pm 0.04					
19 Glycine	1.06 \pm 0.12	4.5 \pm 0.4	3.9 \pm 0.5	1.80 \pm 0.14	$P < 0.0001$	$P < 0.05$	$P < 0.05$	ns	
20 Glycogen	0.11 \pm 0.04	0.19 \pm 0.03	0.18 \pm 0.02	0.03 \pm 0.004	$P < 0.001$	ns	ns	ns	
21 Isoleucine	+	+	+	+					
22 Lactate	1.2 \pm 0.14	1.1 \pm 0.11	1.40 \pm 0.13	0.22 \pm 0.034	$P < 0.0001$	ns	ns	$P < 0.05$	
23 Leucine	+	+	+	+					
24 Lysine	0.43 \pm 0.03	0.2 \pm 0.01	0.19 \pm 0.02	0.22 \pm 0.01	$P < 0.0001$	$P < 0.05$	$P < 0.05$	$P < 0.05$	
25 Methionine	+	+	+	+					
26 Myo-Inositol	1.6 \pm 0.13	3.5 \pm 0.2	1.0 \pm 0.1	0.46 \pm 0.02	$P < 0.0001$	$P < 0.05$	$P < 0.05$	$P < 0.05$	
27 x-N-acetyl	+	+	+	+					
28 Phenylalanine	+	+	+	+					
29 Phosphocholine	0.15 \pm 0.01	0.42 \pm 0.03	0.2 \pm 0.01	0.53 \pm 0.08	$P < 0.0001$	$P < 0.05$	ns	$P < 0.05$	
30 Phosphoethanolamine	+	+	+	+					
31 Proline	+	+	+	+					
32 Sylo-Inositol	0.61 \pm 0.09	1.14 \pm 0.09	0.17 \pm 0.02	0.11 \pm 0.02	$P < 0.0001$	$P < 0.05$	$P < 0.05$	$P < 0.05$	
33 Serine	+	+	+	+					
34 Succinic acid	+	+	ud	+					
35 Taurine	2.2 \pm 0.2	2.6 \pm 0.15	6.8 \pm 0.6	4.06 \pm 0.12	$P < 0.0001$	ns	$P < 0.05$	$P < 0.05$	
36 Threonine	+	+	+	+					
37 Trimethylamine N-oxide	ud	ud	+	+					
38 Tyrosine	+	+	+	+					
39 Valine	0.13 \pm 0.01	0.09 \pm 0.009	0.024 \pm 0.005	0.038 \pm 0.004	$P < 0.0001$	$P < 0.05$	$P < 0.05$	$P < 0.05$	

+, quantification compromised due to low signals and/or overlapping; ns, no significant; ud, undetected.

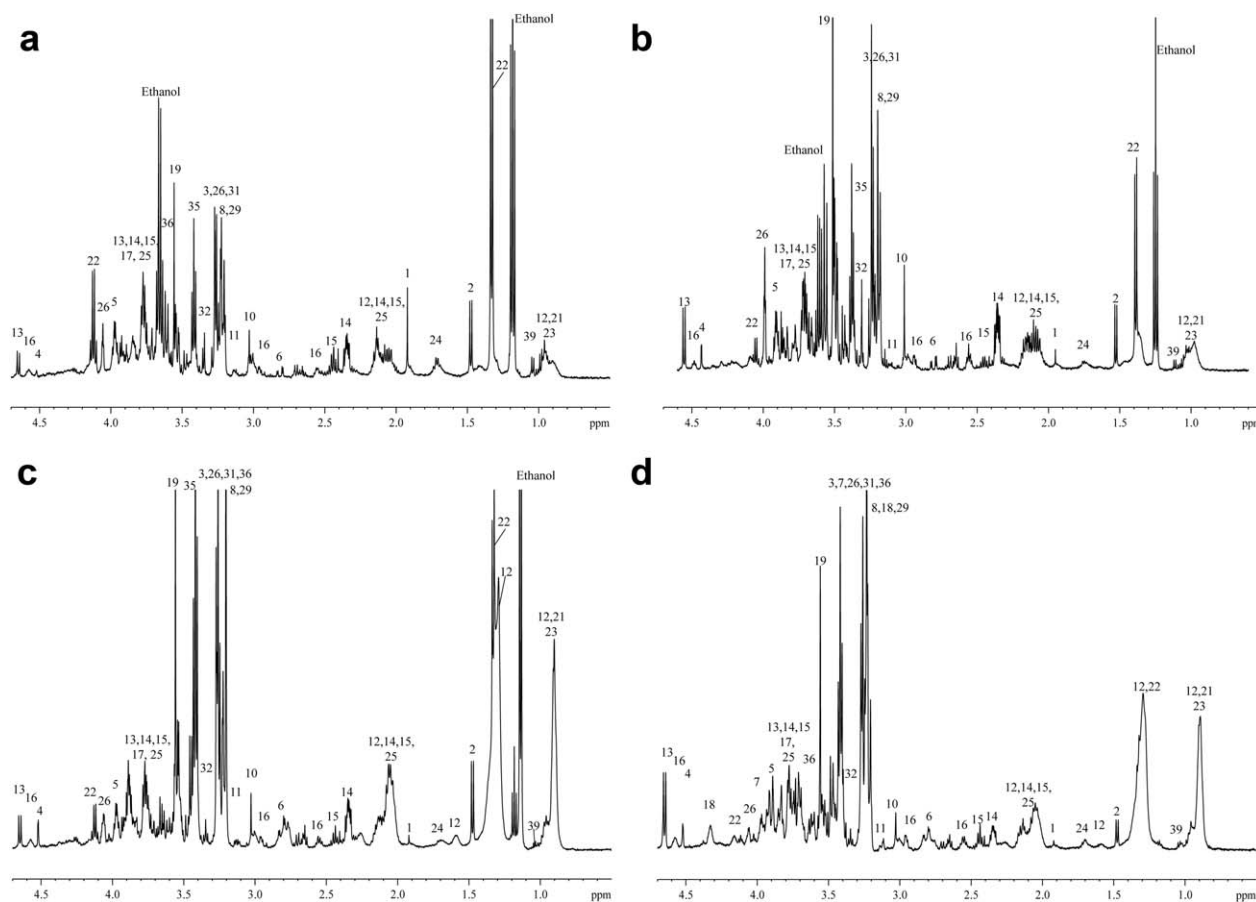


FIG. 1. Representative 1D ^1H CPMG NMR HRMAS spectra performed on lung biopsy samples obtained from humans (a), pigs (b), rats (c), and mice (d). The numbers corresponding to the metabolite assignments are identified in Table 1.

The quantification procedure used here has been described by our team (20). This method is based on a pulse length measurement (pulse length-based concentration). Spectra were normalized according to each sample weight (20). Calibration used the signal intensity of a reference solution containing a known amount of lactate (19.3 nmol), acquired under exactly the same conditions used to measure the biopsy samples. Peak area integration was used to calculate the concentration. For our experiments, only peaks that were well resolved in 1D CPMG spectra were quantified. Chemical shifts for regions of interest were adapted to those of the literature (9,20,22) (Table 2. Fatty acids (a–c) were assigned as described in the literature (25).

Quantification was assessed for 22 metabolites (23 with glycerophosphocholine [GPC] for mice) (Tables 1 and 2). For the remaining metabolites, quantification was compromised due to low signals and/or overlapping.

For some samples, we identified two foreign signals corresponding to ethanol and methanol; this is related to an external contamination from the surgery materials and they were excluded from the quantification.

Statistics

A principal component analysis (PCA) was performed corresponding to an unsupervised multivariate data

reduction routine, which serves to evaluate the quality of the data quickly and to identify possible outliers (26). After the PCA analysis, a partial least-squares discriminant analysis (PLS-DA) (27) is usually used to build a statistical model that optimizes the separation between the two groups using the AMIX 3.8 software (Bruker GmbH, Germany) and SIMCA P (Umetrics AB, Umea, Sweden) (9). The spectral regions between 4.7 ppm and 0.5 ppm of each 1D CPMG NMR were used to define the spectral buckets of 0.01 ppm. An analysis of variance (ANOVA) for repeated measures followed by a Dunnett multicomparison test were performed comparing each metabolite from lung biopsy samples obtained from each animal species to those of human lung biopsy samples.

RESULTS

According to statistical analysis, PCA (three components; $R^2X=0.625$, $Q^2=0.478$) (data not shown) and PLS-DA (three components; $R^2X=0.502$, $Q^2=0.743$) (Fig. 3) human lung was distinguishable from the other groups. The main difference between human and pig tissue is related to component 2 (Fig. 3a), which is due to the variability of metabolite concentrations as will be described below. The composition of the metabolome between human and pig lungs is similar as shown in Figure 3b. This figure also shows that the human metabolome is

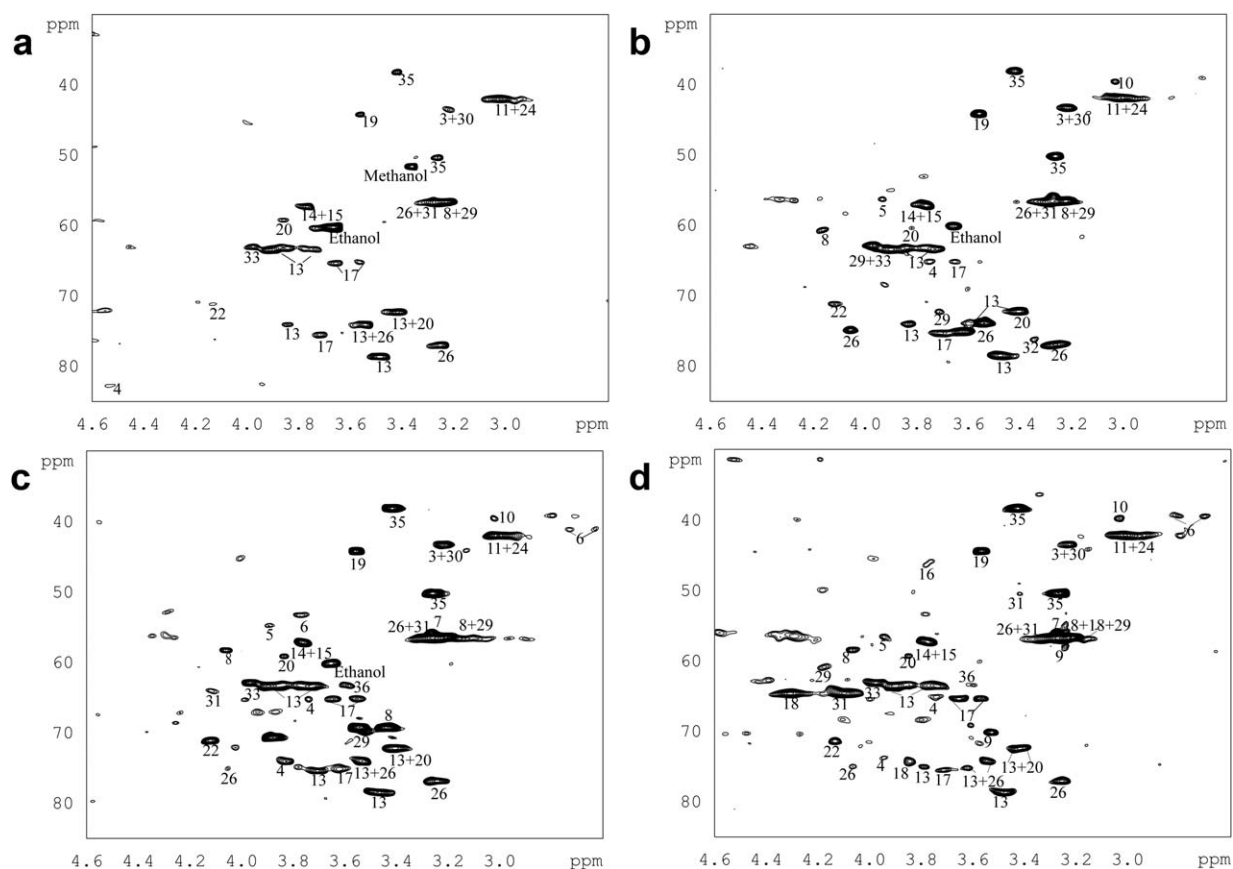


FIG. 2. Representative 2D ^1H - ^{13}C heteronuclear single quantum correlation NMR HRMAS spectra performed on lung biopsy samples obtained from humans (a), pigs (b), rats (c), and mice (d). The numbers corresponding to the metabolite assignments are identified in Table 1. The region selected of ^1H (2.5 ppm–5 ppm) and ^{13}C (30 ppm–85 ppm) being considered the most discriminating region for the metabolite composition. Ethanol and methanol are considered as exogenous contaminants.

clearly separated from rats and mice. On the other hand, the metabolic variability between rats and mice is essentially due to the presence of GPC and carnitine only in mouse lung and to the concentration of glucose, glutamine, and phosphocholine found to be higher in rat lungs. This difference is shown in Figure 3b according to the third component.

Comparison Between Human (Six Humans, $n = 11$) and Mouse (11 Mice, $n = 11$) Tissue

Concerning the mouse lung, the number of identified metabolites reached 39 compared with human lung tissue in which 35 metabolites could be identified. The main differences in metabolite composition consist in: betaine, carnitine, GPC, and trimethylamine *N*-oxide (Figs. 1 and 2 and Table 2), which are present in mouse and not in human lung. Even if GPC was identified in human lung tissues in the publication of Rocha et al. (12), it could not be identified in our lung samples, which may be related to the fact that Rocha's publication focuses on lung cancer tissue. On the other hand, the concentration of total fatty acids (total CH_3) largely exceeds that of human lung (Fig. 1d). Moreover, the PCA analyses (three components; $R^2X = 0.644$, $Q^2 = 0.404$) and PLS-DA (three components; $R^2X = 0.556$, $Q^2 = 0.971$) (data not shown) performed on the total spectra show a

separation between human and mouse lung. In addition, according to the ANOVA followed by the Dunnett test, the significant difference in concentration of metabolites concerns 13 metabolites out of the 22 quantified (Table 1). These 13 metabolites are ascorbic acid, fatty acids, glutathione, phosphocholine, and taurine, whose concentrations increase from twice to three times compared with concentrations in human lung tissue, and acetate, asparagine, glutamate, lactate, lysine, myo-inositol, syllinositol, and valine, whose concentrations are much lower in mouse lung samples than in human lung samples.

Comparison Between Human (Six Humans, $n = 11$) and Rat (11 Rats, $n = 11$) Tissue

The NMR HRMAS experiments identified 36 metabolites from rat lung samples (Table 2) including trimethylamine *N*-oxide and betaine as discriminating metabolites because they are present in rat lung but not in human lung. Conversely, succinic acid was undetected in the rat lung samples. The statistical analysis using PCA (four components; $R^2X = 0.746$, $Q^2 = 0.466$) and PLS-DA (two components; $R^2X = 0.511$, $Q^2 = 0.921$) (data not shown) performed on the total spectra without discrimination show a clear cleavage between human and rat tissues, indicating a difference in the composition of their

Table 2
Resonance Assignments Using 1D ¹H CPMG Spectra and the Integration Range for Each Metabolite Quantified

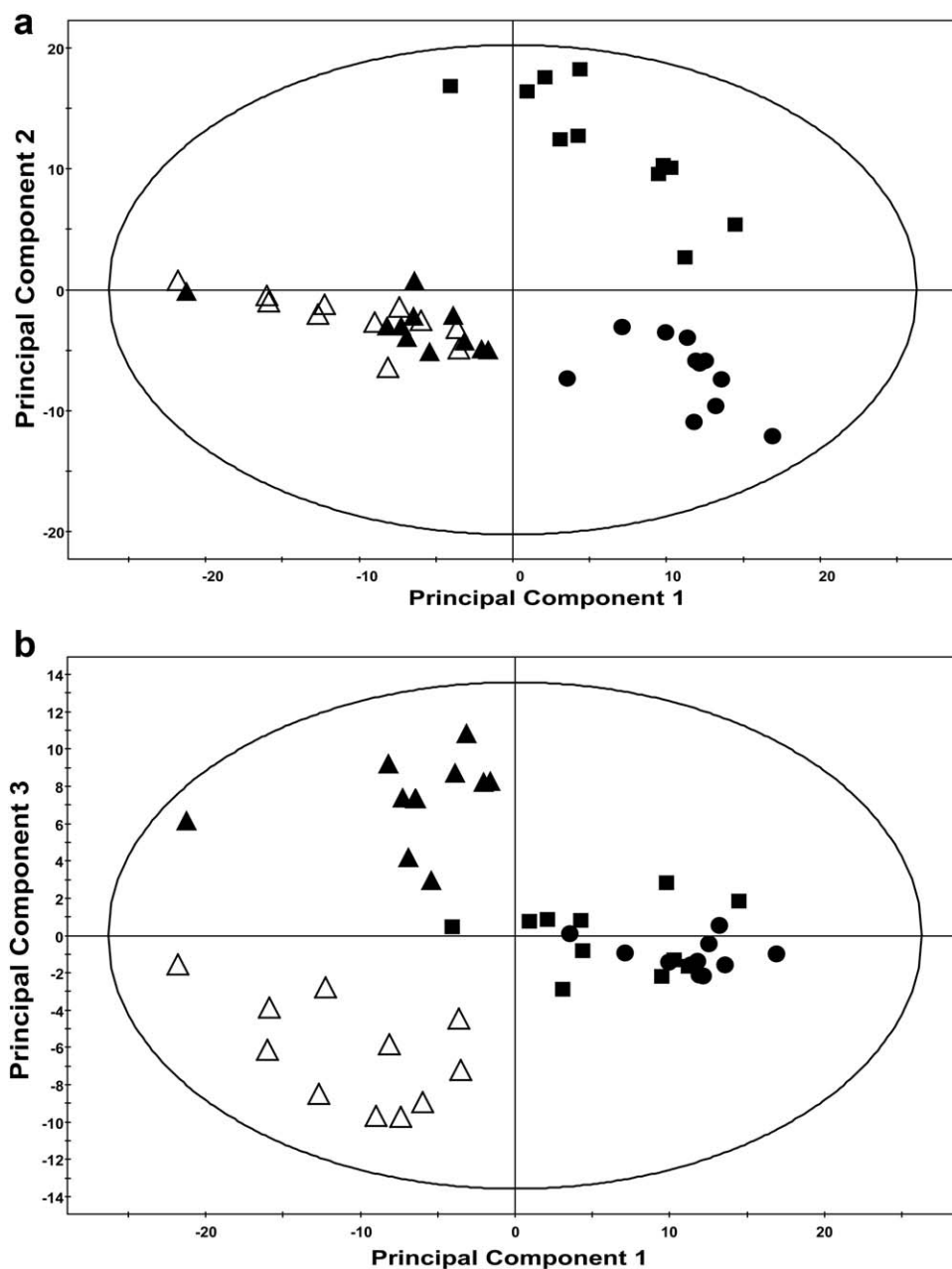
	Compound	Assignment	¹ H chemical shift (ppm)	Integration range (ppm)
1	Acetate	CH3	1.92	[1.914–1.928]
2	Alanine	beta CH3	1.48	[1.460–1.490]
4	Ascorbate	CH2(OH)	4.02	[4.514–4.532]
		C4H	4.52	
5	Asparagine	CH	4	[3.944–4.002]
		CH2	2.94	
		CH2	2.84	
8	Choline	N(CH3)3	3.21	[3.187–3.211]
		CH2	3.52	
		CH2	4.06	
10	Creatine	CH3	3.03	[3.023–3.037]
		CH2	3.93	
11	Ethanolamine	CH2	3.83	[3.103–3.156]
		CH2	3.13	
12	Fatty acid (a)	CH2-1	1.29	[0.800–0.962]
		CH2-2	1.31	
	Fatty acids (a), (b), and (c) ^a	CH3	0.90	
		(n) CH2	1.29	
	Fatty acid (b)	CH2-2	2.03	
		==CH2==	2.8	
		=CH	5.33	
	Fatty acids (a) and (b)	(n) CH2	1.29	
	Fatty acid (c)	CH2-1	2.25	
		CH2-2	1.6	
13	Glucose			[4.630–4.674]
	Alpha glucose	C4H	3.43	
		C1H	5.23	
		C5H	3.84	
	Beta glucose	C3H,C5H	3.47	
		C6H	3.75	
		C6H	3.89	
		C1H	4.65	
14	Glutamate	CH2	2.05	[2.315–2.377]
		CH2	2.34	
		CH	3.76	
15	Glutamine	CH2	2.14	[2.410–2.474]
		CH2	2.44	
		CH	3.77	
16	Glutathione	CH2—CONH	2.54	[2.934–2.974]
		CH—NH2	3.78	
		CH—NH	4.57	
		CH2—SH	2.95	
18	Glycerophosphocholine	N(CH3)3	3.23	[3.228–3.238]
		CH2	4.32	
		CH2	3.69	
		CHOH	3.91	
19	Glycine	CH2	3.55	[3.552–3.570]
20	Glycogen	CH	5.44	[5.411–5.452]
		CH2	3.85	
		CH2	3.79	
		CH	3.43	
		CH	3.60	
22	Lactate	CH3	1.33	[4.097–4.155]
		CH	4.13	
24	Lysine	CH2	1.43	[1.679–1.750]
		CH2	1.71	
		CH2	1.89	
26	Myo-inositol	C5H	3.27	[4.035–4.073]
		C1H·C3H	3.54	
		C4H·C6H	3.61	
		C2H	4.06	

TABLE 2. Continued

	Compound	Assignment	¹ H chemical shift (ppm)	Integration range (ppm)
29	Phosphocholine	N(CH ₃) ₃	3.22	[3.211–3.228]
		CH ₂	3.60	
		CH ₂	4.16	
32	Syllo-inositol	all HS	3.35	[3.388–3.441]
35	Taurine	CH ₂ –NH ₃	3.26	
		CH ₂ –SO ₃	3.42	
38	Tyrosine	CH	3.92	[6.863–6.898]
		CH 3,5	6.87	
		CH 2,6	7.16	
39	Valine	CH ₃	0.98	[1.027–1.055]
		CH ₃	1.04	
		CH	2.30	

^a(a), $-(n)CH_2-(2)CH_2-(1)CH_2-CH_3$; (b), $-CH=CH-CH_2-CH=CH-(2)CH_2-(1)CH_2-(n)CH_2$; (c) $-(n)CH_2-(2)CH_2-(1)CH_2-COOH$.

FIG. 3. Three component PLS-DA model obtained when classifying the entire experiments performed on lung biopsies obtained from humans, pigs, mice, and rats ($n = 55$) using the 4.7–0.5 ppm spectral region ($R^2X = 0.502$, $Q^2 = 0.743$). **a**: The PLS-DA according to the principal component 1 and the principal component 2 and **(b)** represents the PLS-DA according to the principal component 1 and the principal component 3. Full box: human; Full circle: pig; Full triangle: rat; Open triangle: mouse.



metabolome. Furthermore, we noted a number of differences in the concentration of the major metabolites, which is confirmed by the ANOVA test (Table 1) because 16 metabolites of the 22 quantified show a significant difference. In addition, the fatty acids are highly elevated in rat lung as compared with human lung (Table 1) (Fig. 1c).

Comparison Between Human (Six Humans, $n = 11$) and Pig (Seven Pigs, $n = 11$) Tissue

The NMR-based metabolomics experiments performed on lung from pigs and humans identified 35 metabolites (Table 2) in both human and pig tissues, indicating their similar metabolome (Figs. 1 and 2). However, regarding the statistical analysis of the PLS-DA (two components; $R^2X = 0.522$, $Q^2 = 0.896$) (data not shown), a clear separation between the two groups (human and pig samples) appears. Moreover, following the quantification of 23 metabolites and performing the ANOVA followed by the Dunnett test, we noted a significant difference in concentrations of 14 discriminating metabolites among the 22 quantified metabolites (Table 2), indicating that the main differences concern the concentration of some metabolites and not the composition of the metabolome. Indeed, for ascorbic acid, creatine, glutamate, glutathione, lysine, myo-inositol, phosphocholine, and sylo-inositol, we noted that their concentration in pig lung is almost twice that of the human lung and fourfold for glycine. Conversely, the concentration of other metabolites such as glucose, glutamine, and valine is higher in human than in pig lung.

DISCUSSION

The metabolomics by NMR HRMAS spectroscopy allows the study of intact biopsy samples in order to identify biomarkers. It has become increasingly useful in the study of several diseases. However, very few papers in the literature combine the use of metabolomics and the assessment of the metabolic content of lung tissue (9,12). We here assessed the metabolome of lung biopsy samples of various animal species, i.e., pig, mouse, and rat as compared with human.

The NMR HRMAS spectra were acquired with a short duration of 20 min and under moderate sample spinning (3 kHz), enabling us to obtain a reliable quantification. Because it was shown that the rotation of the sample to 5 kHz during a short period of time does not lead to significant deterioration of the tissue (28).

According to statistical data described above, human lung was distinguishable from the other animal species. However, the main difference observed between human and pig tissues concern the concentration of some metabolites and not the composition of the metabolome. This may explain the differences noticed between Figure 2A,B; this is only due to the spectral resolution related to the concentration of certain metabolites, which differs from one species to another. Nonetheless, even when the ANOVA test shows a significant difference between human and pig lung, we noted that concentrations were very similar indicating their close metabolic composition. These results are in agreement with the choice of

pig as an animal model in lung transplantation studies. Indeed, typically pig is used as the optimal animal model for surgery experimentations and functional lung measurements (9,29–31); this is related to the pulmonary physiological characteristics close to humans.

Concerning the rodents, human lung was distinguishable from mouse and rat regarding: trimethylamine *N*-oxide and betaïne (18,32), which were present in rodents but not in human lung, carnitine, and GPC (19) which were present in mouse but not in human lung. Conversely, succinic acid was undetected in rat lung (32). In addition to the differences in the metabolic composition, there is an important difference in metabolite concentrations. Indeed, fatty acids concentration was significantly higher in rodent lungs compared with human lung. Nevertheless, even if the number of discriminating metabolites (13 metabolites) appears lower in mice, the difference in concentration is greater with respect to the comparison with the other species. These results clearly indicate a large difference in the lung metabolome of rodent tissues compared with that of human tissue.

CONCLUSIONS

This comparative study aimed at identifying the closest animal species to human with regards to lung tissue. Using the metabolomics, NMR HRMAS directly on lung biopsy samples allowed to highlight that pig lung seems close to human lung as regarding its metabolite composition with more similarities than dissimilarities.

REFERENCES

- Patti GJ, Yanes O, Siuzdak G. Innovation: metabolomics: the apogee of the omics trilogy. *Nat Rev Mol Cell Biol* 2012;13:263–269.
- Nicholson JK, Connelly J, Lindon JC, Holmes E. Metabolomics: a platform for studying drug toxicity and gene function. *Nat Rev Drug Discov* 2002;1:153–161.
- Lindon JC, Beckonert OP, Holmes E, Nicholson JK. High-resolution magic angle spinning NMR spectroscopy: application to biomedical studies. *Prog Nucl Mag Res Spectrosc* 2009;55:79–100.
- Bertini I, Cacciatore S, Jensen BV, Schou JV, Johansen JS, Kruhoffer M, Luchinat C, Nielsen DL, Turano P. Metabolomic NMR fingerprinting to identify and predict survival of patients with metastatic colorectal cancer. *Cancer Res* 2012;72:356–364.
- Griffin JL, Shockcor JP. Metabolic profiles of cancer cells. *Nat Rev Cancer* 2004;4:551–561.
- Bathen TF, Sitter B, Sjøbakk TE, Tessem M-B, Gribbestad IS. Magnetic resonance metabolomics of intact tissue: a biotechnological tool in cancer diagnostics and treatment evaluation. *Cancer Res* 2010;70:6692–6696.
- Hassan-Smith G, Wallace GR, Douglas MR, Sinclair AJ. The role of metabolomics in neurological disease. *J Neuroimmunol* 2012;248:48–52.
- Bain JR, Stevens RD, Wenner BR, Ilkayeva O, Muoio DM, Newgard CB. Metabolomics applied to diabetes research. *Diabetes* 2009;58:2429–2443.
- Benahmed MA, Santelmo N, Elbayed K, et al. The assessment of the quality of the graft in an animal model for lung transplantation using the metabolomics ^1H high-resolution magic angle spinning NMR spectroscopy. *Magn Reson Med* 2012;68:1026–1038.
- Stenlund H, Madsen R, Vivi A, Calderisi M, Lundstedt T, Tassini M, Carmellini M, Trygg J. Monitoring kidney-transplant patients using metabolomics and dynamic modeling. *Chemomet Intell Lab* 2009;98:45–50.
- Duarte LF, Stanley EG, Holmes E, et al. Metabolic assessment of human liver transplants from biopsy samples at the donor and recipient stages using high-resolution magic angle spinning ^1H NMR spectroscopy. *Anal Chem* 2005;77:5570–5578.

12. Rocha CM, Barros AS, Gil AM, et al. Metabolic profiling of human lung cancer tissue by ^1H high-resolution magic angle spinning (HRMAS) NMR spectroscopy. *J Proteome Res* 2010;1:319–332.
13. Rocha CM, Carrola J, Barros AS, et al. Metabolic signatures of lung cancer in biofluids: NMR-based metabolomics of blood plasma. *J Proteome Res* 2011;10:4314–4324.
14. Ubhi BK, Riley JH, Shaw PA, Lomas DA, Tal-Singer R, MacNee W, Griffin JL, Connor SC. Metabolic profiling detects biomarkers of protein degradation in COPD patients. *ERJ Express* 2012;40:345–355.
15. Saude EJ, Skappak CD, Regush S, Cook K, Ben-Zvi A, Becker A, Moqbel R, Sykes BD, Rowe BH, Adamko DJ. Metabolomic profiling of asthma: diagnostic utility of urine nuclear magnetic resonance spectroscopy. *J Allergy Clin Immunol* 2011;127:757–764.
16. Jayle C, Corbi P, Eugene M, Carretier M, Hebrard W, Menet E, Hauet T. Beneficial effect of polyethylene glycol in lung preservation: early evaluation by proton nuclear magnetic resonance spectroscopy. *Ann Thorac Surg* 2003;76:896–902.
17. Griffin JL. Understanding mouse models of disease through metabolomics. *Curr Opin Chem Biol* 2006;10:309–315.
18. Serkova NJ, Van Rheen Z, Tobias M, Pitzer JE, Wilkinson JE, Stringer KA. Utility of magnetic resonance imaging and nuclear magnetic resonance-based metabolomics for quantification of inflammatory lung injury. *Am J Physiol Lung Cell Mol Physiol* 2008;295:L152–L161.
19. Ji-Hyun S, Ji-Young Y, Bo-Young J, Yoo Jeong Y, Sang-Nae C, Yeon-Ho K, Do Hyun R, Geum-Sook H. ^1H NMR-based metabolomic profiling in mice infected with *Mycobacterium tuberculosis*. *J Proteome Res* 2011;10:2238–2247.
20. Piotta M, Moussallieh FM, Imperiale A, Benahmed MA, Detour J, Belloq JP, Namer IJ, Elbayed K. Reproducible sample preparation and spectrum acquisition techniques for metabolic profiling of human tissues by ^1H HRMAS NMR. In Lutz P, editor. *Methodologies in metabolomics: experimental strategies and techniques for metabolomics research*. Cambridge, UK: Cambridge University Press; 2012. pp 496–524.
21. Opstad KS, Bell BA, Griffiths JR, Howe FA. An assessment of the effects of sample ischaemia and spinning time on the metabolic profile of brain tumour biopsy specimens as determined by high-resolution magic angle spinning ^1H NMR. *NMR Biomed* 2008;21:1138–1147.
22. Detour J, Elbayed K, Piotta M, Moussallieh FM, Nehlig A, Namer IJ. Ultrafast in vivo microwave irradiation for enhanced metabolic stability of brain biopsy samples during HRMAS NMR analysis. *J Neurosci Methods* 2011;201:89–97.
23. Elbayed K, Dillmann B, Raya J, Piotta M, Engelke F. Field modulation effects induced by sample spinning: application to high-resolution magic angle spinning NMR. *J Magn Reson* 2005;174:2–26.
24. Bathen, TF, Jensen, LR, Sitter B, Fjösne HE, Halgunset J, Axelson DE, Gribbestad IS, Lundgren S. MR-determined metabolic phenotype of breast cancer in prediction of lymphatic spread, grade, and hormone status. *Breast Cancer Res Treat* 2007;104:181–189.
25. Martínez-Bisbal MC, Martí-Bonmatí L, Piquer J, Revert A, Ferrer P, Llácser JL, Piotta M, Assemat O, Celda B. ^1H and ^{13}C HR-MAS spectroscopy of intact biopsy samples ex vivo and in vivo ^1H MAS study of human high grade gliomas. *NMR Biomed* 2004;17:191–205.
26. Ebbels TMD, Cavill R. Bioinformatic methods in NMR-based metabolic profiling. *Prog Nucl Mag Res Spectrosc* 2009;55:361–374.
27. Wold S, Sjöström M, Eriksson L. PLS-regression: a basic tool of chemometrics. *Chemomet Intell Lab* 2001;58:109–130.
28. Cheng LL, Louis DN, Gonzalez RG. Correlation of high-resolution magic angle spinning proton magnetic resonance spectroscopy with histopathology of intact human brain tumor specimens. *Cancer Res* 1998;58:1825–1832.
29. Jayle C, Hauet T, Menet E, Hébrard W, Hameury F, Eugene M, Carretier M, Corbi P. Beneficial effects of polyethylene glycol combined with low-potassium solution against lung ischemia/reperfusion injury in an isolated, perfused, functional pig lung. *Transplant Proc* 2002;34:834–835.
30. Jayle C, Corbi P, Eugene M, Carretier M, Hebrard W, Menet E, Hauet T. Beneficial effect of polyethylene glycol in lung preservation: early evaluation by proton nuclear magnetic resonance spectroscopy. *Ann Thorac Surg* 2003;76:896–902.
31. Pizanis N, Petroy A, Heckmann J, Wiswedel I, Wohlschläger J, de Groot H, Jakob H, Rauen U, Kamler MA. New preservation solution for lung transplantation: evaluation in a porcine transplantation model. *J Heart Lung Transplant* 2012;31:310–317.
32. Jiang L, Huang J, Wang Y, Tang H. Metabonomic analysis reveals the CCl_4 -induced systems alterations for multiple rat organs. *J Proteome Res* 2012;11:3848–3859.